ACCSCIENCE PUBLISHING

International Journal of Bioprinting

RESEARCH ARTICLE

3D-bioprinted asymmetric bilayer scaffolds with anti-infection and pro-regeneration characteristics for chronic diabetic wound healing

Chenyu Zhang[1,2,3†], Yuan Fang[4†], Lei Pan[5†], Hongyu Chen[2,3], Yu Han[6], Qiang Wu[2,3], Ye Sun[7], Quan Hu[8*], Zuyan Lu[2,3*], Yongqiang Hao[2,3*], and Yuanyuan Liu[1*]

[1]School of Medicine, Shanghai University, Shanghai, China

[2]Shanghai Key Laboratory of Orthopaedic Implants, Department of Orthopaedic Surgery, Shanghai Ninth People's Hospital, Shanghai Jiao Tong University School of Medicine, Shanghai, China

[3]Clinical and Translational Research Center for 3D Printing Technology, Shanghai Ninth People's Hospital, Shanghai Jiao Tong University School of Medicine, Shanghai, China

[4]Department of Plastic and Reconstructive Surgery, Shanghai Ninth People's Hospital, Shanghai Jiao Tong University School of Medicine, Shanghai, China

[5]Nursing Department, Ren Ji Hospital, School of Medicine, Shanghai Jiao Tong University, Shanghai, China

[6]Department of Orthopaedics, Medical 3D Printing Center, The First Affiliated Hospital of Zhengzhou University, Zhengzhou, Henan, China

[7]Department of Orthopedics, The First Affiliated Hospital of Nanjing Medical University, Nanjing, Jiangsu, China

[8]Department of Burns and Plastic Surgery, The Fourth Medical Center of Chinese PLA General Hospital, Beijing, China

[†]*These authors contributed equally to this work.*

***Corresponding authors:**
Yuanyuan Liu
(yuanyuan_liu@shu.edu.cn)
Yongqiang Hao
(haoyq1664@sh9hospital.org.cn)
Zuyan Lu
(l91z03y09@hotmail.com)
Quan Hu
(huquan304@163.com)

Citation: Zhang C, Fang Y, Pan L, *et al*. 3D-bioprinted asymmetric bilayer scaffolds with anti-infection and pro-regeneration characteristics for chronic diabetic wound healing. *Int J Bioprint*. 2026:12(2):026120099. doi: 10.36922/IJB026120099

Received: March 17, 2026

Revised: April 6, 2026

Accepted: April 8, 2026

Published online: April 22, 2026

(This article belongs to the *Special Issue: 3D Printing in Clinical Application*)

Abstract

Chronic diabetic wounds, characterized by persistent infection and impaired tissue regeneration, remain a formidable clinical challenge. In the present study, a 3D-bioprinted asymmetric bilayer scaffold was developed by integrating electrospinning and 3D bioprinting technologies to achieve anti-infective and pro-regenerative functions. The scaffold features a distinctive asymmetric architecture comprising a superficial layer (Layer S) and a basal layer (Layer B). Layer B, consisting of electrospun copper(I) oxide (Cu_2O)–poly-ε-caprolactone nanofibers, serves as an effective antibacterial barrier specifically targeting methicillin-resistant *Staphylococcus aureus* (MRSA), while Layer S employs a 3D-bioprinted decellularized extracellular matrix hydrogel loaded with human bone marrow mesenchymal stem cell-derived extracellular vesicles (hBMSC-EVs) to facilitate tissue repair. Experimental results demonstrated that hBMSC-EVs significantly augmented fibroblast proliferation and migration, and the Cu_2O-doped layer exhibited potent bactericidal activity against MRSA. In db/db diabetic mice, this asymmetric composite scaffold significantly accelerated wound closure compared to standalone treatments. Histological analysis further confirmed enhanced neovascularization and accelerated extracellular matrix reconstruction. Overall, this synergistic 3D-bioprinted bilayer system provides a

high-performance strategy for the targeted management of MRSA-infected chronic diabetic wounds.

Keywords: Diabetic wound healing; 3D bioprinting; Extracellular vesicles; Decellularized extracellular matrix; Electrospinning; Antibacterial scaffold

1. Introduction

Maintaining skin structural integrity is crucial for normal physiological function, but chronic non-healing wounds pose a significant challenge in the medical field.[1,2] These wounds, defined as lesions that do not heal within a four-week period, are particularly problematic in individuals with metabolic disorders such as diabetes mellitus. Among these, diabetic foot ulcers (DFUs) represent the most common and clinically burdensome subtype, accounting for approximately 50% to 70% of all non-healing wound cases,[3] and are responsible for over 80% of non-traumatic lower-limb amputations.[4] It is estimated that 15% to 25% of diabetic patients will develop a DFU in their lifetime. DFUs are characterized by deep tissue involvement, spatial variability, and heightened susceptibility to multidrug-resistant bacterial infections.[5,6] In China alone, there are more than 30 million cases of severe surface wounds reported each year, putting a heavy strain on healthcare resources.[7,8]

Physiologically, chronic diabetic wounds represent a pathological stalemate. Although hyperglycemia is a systemic driver, impaired healing is sustained locally by persistent infection and impaired angiogenesis.[9] These wounds are characterized by deep tissue involvement and spatial variability, which conventional dressings often fail to address. Consequently, there is an urgent demand for "smart" dressings that can simultaneously provide an antibacterial barrier, a biomimetic 3D architecture, and potent cues for vascular remodeling.[10-12]

To address these complex requirements, the integration of electrospinning and 3D bioprinting offers a transformative approach to scaffold design.[13-16] Unlike traditional dressings that simply serve as barriers, this combined manufacturing approach allows for precise customization of porosity to facilitate gas exchange, while also replicating the structural characteristics of the natural extracellular matrix (ECM).[17-23] Specifically, the controllable alignment of electrospun fibers provides spatial chemotactic cues that accelerate re-epithelialization, whereas 3D-bioprinted structures offer the mechanical integrity needed for deep tissue repair.[24,25]

The efficacy of regenerative scaffolds is significantly improved by incorporating biological cues, specifically extracellular vesicles (EVs) derived from human bone marrow mesenchymal stem cells (hBMSCs) (hBMSC-EVs).[26-29] hBMSCs play a pivotal role in tissue remodeling via paracrine effects, releasing EVs that modulate inflammatory cascades, promote microvascular tube formation, and suppress excessive fibrosis.[30] By combining these bioactive components with a decellularized skin extracellular matrix (dSEM) hydrogel, a highly compatible microenvironment is created that closely resembles the natural wound environment. This unique combination offers a distinct advantage for promoting the swift and scarless healing of complex diabetic wounds.[31,32]

In the present study, we developed an innovative asymmetric bilayer composite biomimetic scaffold designed to simultaneously address infection and tissue repair. The scaffold was designed with dual functions, comprising a base copper(I) oxide (Cu_2O)-doped antibacterial layer and a top regenerative dSEM-based hydrogel layer incorporating hBMSC-derived EVs. These hBMSC-derived EVs facilitate endogenous cell recruitment and accelerate healing.

Evaluation in a diabetic mouse model—a challenging environment characterized by impaired wound healing—demonstrated the superior therapeutic efficacy of this composite scaffold. By integrating the potent antibacterial properties of Cu_2O with the pro-regenerative effects of dSEM-EVs, this approach provides a high-performance solution for managing complex diabetic wounds. Our findings suggest that this synergistic strategy effectively drives the healing cascade in dysregulated metabolic conditions, offering a promising clinical alternative for chronic wound care.

2. Materials and methods

2.1. Preparation and characterization of hBMSC-EVs and 3D-printed dSEM-EV scaffolds

2.1.1. Preparation and characterization of hBMSC-EVs

Human bone marrow mesenchymal stem cells (hBMSCs) were acquired from the cell bank of the Chinese Academy of Sciences, Shanghai, China. When the hBMSCs reached 70% confluence, the culture medium (Senkicel,

China) was replaced with a serum-free medium for hBMSC-EV isolation. This extraction process involved ultracentrifugation (Optima LE-80 K, Beckman Coulter, United States of America [USA]) at 100,000× g and 4 °C for a duration of 90 min.

The isolated EVs were characterized morphologically using transmission electron microscopy (TEM; BIOTWIN, FEI, USA), and their size distribution was analyzed by nanoparticle tracking analysis (NTA; Nanosight NTA v3.2, Malvern, United Kingdom) after a 1:1,000 dilution with phosphate-buffered saline. For visualization of cellular uptake, the EVs were labeled with PKH26 fluorescent dye (Sigma-Aldrich, USA). Western blotting was performed to confirm the expression of EV-specific surface markers such as CD9, TSG101, and HSP70, and the absence of the negative marker calnexin.

2.1.2. In vitro evaluation of hBMSC-EV bioactivity

The effects of hBMSC-EVs at concentrations of 3, 30, and 300 μg/mL on fibroblast proliferation and migration were evaluated using 3T3 cells (Procell, China). Cell proliferation was assessed using a CCK-8 assay (Beyotime, China). For the scratch test, cells were seeded in 6-well plates and cultured until they reached approximately 100% confluence. A straight scratch was manually created in the cell monolayer using a sterile pipette tip. The wells were then washed three times with phosphate-buffered saline (PBS) to remove detached cells and debris. The cells were subsequently incubated in serum-free medium, and images of the scratch area were captured at 48 and 96 h. The wound area was quantified using ImageJ software (1.42, NIH, USA). The viability of the cells inside the dSEM-EV was detected through the CAM/PI Live/Dead staining kit (Invitrogen, Thermofisher, USA). The 10% GelMA hydrogel (GM60, EFL, China) and 4.5 mg/mL collagen hydrogel (Cebrary, Yeasen, China) were used as the control group.

2.1.3. Preparation and characterization of the 3D-printed dSEM-EV scaffolds

Human skin tissue was obtained clinically, transported in sterile culture medium, and decellularized utilizing 0.25% trypsin and 70% ethanol for 16 h to prepare dSEM. Concurrently, the intrinsic matrix composition was qualitatively and quantitatively profiled via liquid chromatography–mass spectrometry (LC-MS)-based proteomics.

For the preparation and characterization of a printable dSEM-EV scaffold, the lyophilized dSEM powder was solubilized under continuous stirring for 48 h. Based on our established protocols, a dSEM-EV bio-ink was neutralized and formulated at optimized volumetric ratios of dSEM hydrogel (6 mg/mL) and hBMSC-EVs (300 μg/mL).[22] After printing, the dSEM-EV scaffold was incubated and crosslinked at 37 °C for 1 h, based on our previous protocol.[22] The rheological properties of the prepared bio-ink were systematically characterized by HR-2 Discovery rheometer (TA Instruments, USA) to confirm its printability and structural fidelity. Subsequently, an integrated 3D bioprinting system (Bio-Printer-WS, Regenove, China) was employed to fabricate the dSEM-EV scaffold at a printing speed of 3 mm/s by extruding and stacking the hydrogel in a layer-by-layer manner.

2.1.4. Cytocompatibility and protein release of the dSEM-EV scaffolds

Cell viability within the dSEM-EV scaffold was evaluated using a Calcein-AM/propidium iodide (CAM/PI) Live/Dead staining kit (Invitrogen, Thermo Fisher, USA). A 10% GelMA hydrogel (GM60, EFL, China) and a 4.5 mg/mL collagen hydrogel (Cebrary, Yeasen, China) were used as control groups. The protein release profile of the scaffold was quantified on days 1, 3, 5, and 7 using a BCA protein assay kit (Thermo Fisher, USA).

2.2. Fabrication and evaluation of anti-infection and pro-regeneration properties of the composite scaffold

2.2.1. Fabrication of electrospun nanofibrous scaffolds and evaluation of anti-infection performance

Initially, PCL solutions (60,000 Mw; Sigma, USA) incorporating varying concentrations of Cu_2O nanoparticles (Sigma, USA) were prepared. The mixture was then extruded through the polymer extruder (SJ25, Orotrim, China) and cooled to form granules. Subsequently, composite nanofibers with distinct diameters, spatial alignments, and porosities were fabricated using a 3D electrospinning machine (TL-Direct Writing 150, Tongli, China) at a voltage of 6 kV, a printing speed of 1,500 mm/min, and a barrel temperature of 65 °C.[33] The mechanical tensile strength of the scaffolds was evaluated using a universal materials testing machine (5969, Instron, USA). The surface elemental composition and oxidation state of copper were analyzed by X-ray photoelectron spectroscopy (XPS; K-Alpha, Thermo Scientific, USA). The surface morphology and pore distribution of the PCL/Cu_2O composite fibers were assessed utilizing scanning electron microscopy (SEM; Gemini 360, Zeiss, Germany). The surface wettability of the scaffolds was evaluated by water contact angle measurement using the sessile drop method (JC 2000D2H, China). The antimicrobial efficacy of the nanofibrous scaffolds was determined by the CAM/

PI Live/Dead staining kit (Invitrogen, Thermofisher, USA). In addition, a zone of inhibition assay was performed using the Kirby–Bauer disk diffusion method. The diameters of the inhibitory zones against methicillin-resistant *Staphylococcus aureus* (MRSA) cultured on agar plates were measured and recorded to assess the scaffold's antibacterial activity against drug-resistant pathogens.

2.2.2. Fabrication of the bilayer composite scaffolds

A hybrid electrospinning and 3D bioprinting approach was utilized to fabricate the superficial layer (Layer S) and the basal layer (Layer B) of the dermal scaffold. Layer S was engineered with a fiber spacing of 300 μm, an intersecting angle of 90°, and a defined thickness of 50 μm. Layer B was constructed with a filament diameter of 200 μm, a spacing of 100 μm, an intersecting angle of 0°/90°, and a thickness of 3 mm, ultimately yielding a structurally integrated monolithic bilayer composite scaffold.

2.2.3. Establishment of the animal wound model and evaluation of healing

Twenty-four male db/db diabetic mice were utilized to establish a circular full-thickness skin defect model on the dorsum under continuous gas anesthesia. The animals were subsequently randomly assigned to different treatment groups (four groups, $n = 6$ animals per group) to receive corresponding interventions. Macroscopic photographs of the wounds were taken on postoperative days 5, 10, 15, and 20. Upon completion of the observation period, the regenerative skin tissues at the wound sites were harvested, fixed in paraformaldehyde, embedded in paraffin, and sectioned. These sections were subsequently stained with hematoxylin and eosin (H&E) and Masson's trichrome and subjected to immunohistochemical staining for histological evaluation of the healing cascade.

2.2.4. Differential gene expression and functional enrichment analysis

Differential gene expression analysis was performed using R packages to identify significantly altered genes. Functional enrichment analysis was then conducted for Gene Ontology categories, including biological process (BP), cellular component (CC), and molecular function (MF), as well as Kyoto Encyclopedia of Genes and Genomes (KEGG) pathways.

2.2.5. RT-qPCR analysis

For quantitative real-time polymerase chain reaction (RT-qPCR) analysis, total RNA was isolated using an RNeasy Mini Kit (QIAGEN, USA). All qPCR experiments were performed on a QuantStudio 3 PCR System (Thermo Fisher Scientific, USA).

2.3. Statistical analysis

Statistical analyses were performed using GraphPad Prism (XXX, Graphpad, USA) and SPSS (XXX, IBM, USA). Quantitative data are presented as mean ± standard deviation. Differences between two groups were assessed using Student's *t*-test. Comparisons among more than two groups at a single time point were performed using one-way ANOVA followed by an appropriate post hoc test. For wound-healing data measured across multiple postoperative time points, a two-way ANOVA/repeated-measures analysis was performed as appropriate. A p-value of less than 0.05 was considered statistically significant.

3. Results

3.1. Isolation, characterization, and cellular internalization of hBMSC-EVs

To establish the biological foundation of the pro-regenerative scaffold, hBMSC-EVs were successfully isolated via differential ultracentrifugation. Morphological evaluation using TEM revealed that the isolated hBMSC-EVs exhibited a typical cup-shaped or spherical bilayer vesicular structure (Figure 1A). NTA further confirmed that the hydrodynamic diameter distribution of the EVs was highly homogeneous, predominantly concentrated within the expected nanoscale range (approximately 100–200 nm) (Figure 1B). To confirm the cellular uptake capacity, hBMSC-EVs were fluorescently labeled with PKH26 (Figure 1C). Furthermore, Western blot analysis verified the robust expression of EV-specific positive surface markers (CD9, TSG101, HSP70), and the absence of expression of EV-specific negative surface markers calnexin (Figure 1D), thereby validating the high purity of the isolated vesicular fraction. Subsequent *in vitro* co-culture assays demonstrated that the PKH26-labeled EVs were efficiently internalized by the target mesenchymal stem cells, accumulating predominantly in the perinuclear region.

3.2. Bioactivity of hBMSC-EVs on fibroblast cell proliferation and migration

The regenerative potential of the isolated hBMSC-EVs was evaluated *in vitro*. Cell viability and proliferation assessments revealed that the administration of hBMSC-EVs significantly augmented the proliferative capacity of fibroblast cells (3T3 cells) in a concentration-dependent manner, with the highest concentration group exhibiting the most pronounced metabolic activity ($p < 0.0001$) (Figure 1E). Furthermore, the *in vitro* scratch wound healing assay corroborated these findings. Compared to the untreated control group, cells treated with hBMSC-EVs demonstrated accelerated migratory behavior and

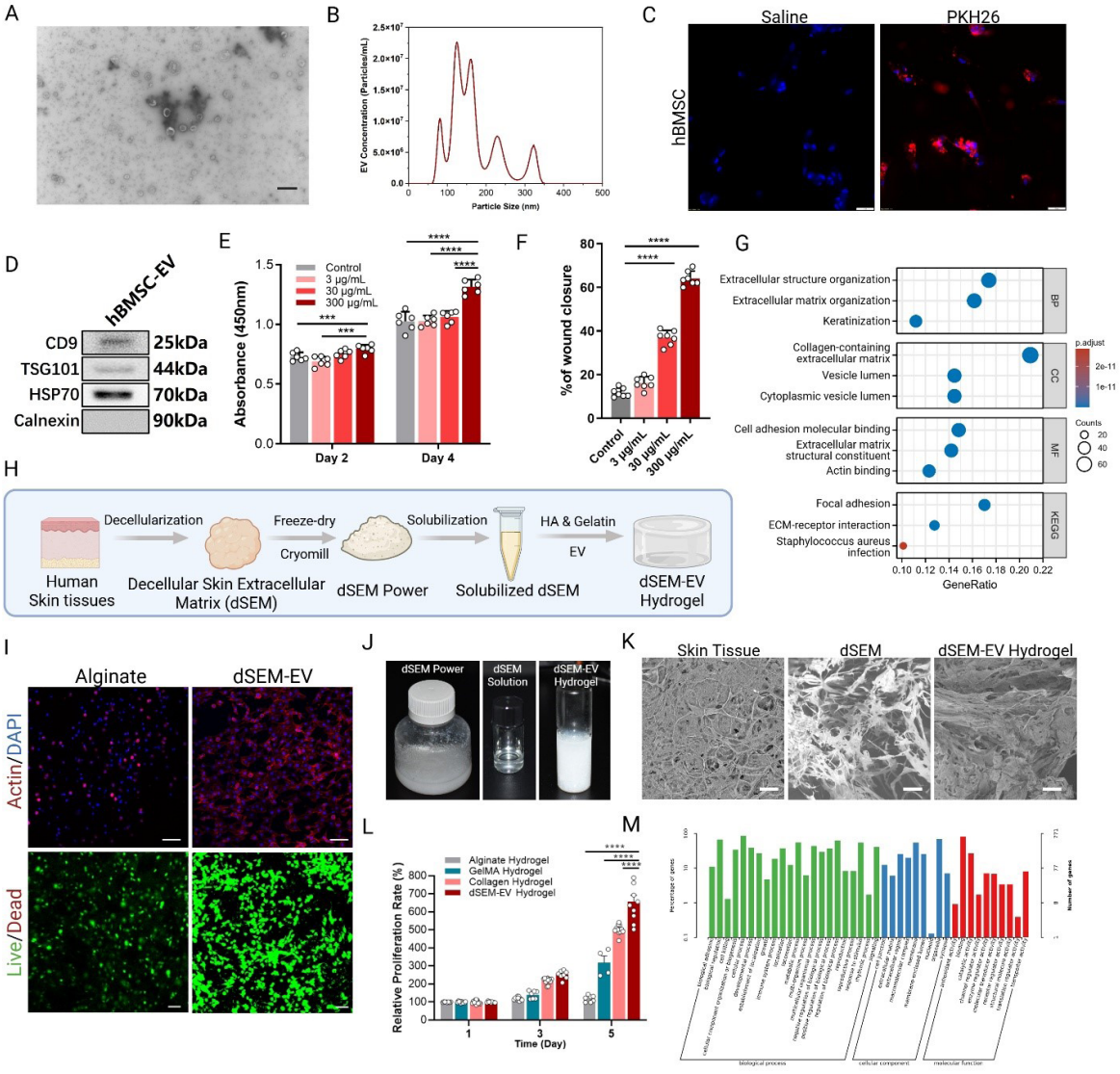

Figure 1. Characterization of human bone marrow mesenchymal stem cell-derived extracellular vesicles (hBMSC-EVs) and the biomimetic decellularized skin extracellular matrix-hyaluronic acid (dSEM-HA) composite hydrogel, and evaluation of their *in vitro* bioactivities. (A) Representative transmission electron microscopy image of hBMSC-EVs showing typical cup-shaped morphology. Scale bars: 500 nm; magnification: 18,500×. (B) Particle size distribution and concentration of BMSC-EVs as determined by nanoparticle tracking analysis (n = 3). (C) Immunofluorescence images demonstrating the cellular internalization of PKH26-labeled hBMSC-EVs (red) by recipient cells. Nuclei were counterstained with DAPI (blue). Scale bars: 50 μm; magnification: 400×. (D) Western blot analysis of EV-specific positive markers (CD9, TSG101, and HSP70) and the negative marker (calnexin). (E) Cell proliferation assessment via CCK-8 assay following treatment with gradient concentrations of hBMSC-EVs (3, 30, and 300 μg/mL) at days 2 and 4 (n = 4). (F) Quantitative analysis of the wound closure rate in an *in vitro* scratch assay under different hBMSC-EV concentrations (n = 6). (G) Bubble chart displaying Gene Ontology (GO) and Kyoto Encyclopedia of Genes and Genomes (KEGG) pathway enrichment analysis based on liquid chromatography–mass spectrometry proteomics of the dSEM. (H) Schematic illustration of the extraction and fabrication workflow for dSEM powder and the subsequent dSEM-EV hydrogel. (I) Representative fluorescence images showing cytoskeletal morphology (actin/DAPI, top) and cell viability (Live/Dead staining, bottom) of cells encapsulated within alginate and dSEM-EV hydrogels. Scale bars: 100 μm; magnification: 200×. (J) Macroscopic photographs of the lyophilized dSEM powder, solubilized dSEM precursor, and the final formulated dSEM-EV hydrogel. (K) Scanning electron microscopy micrographs illustrating the microstructural topology of native skin tissue, porous dSEM, and the crosslinked dSEM-EV hydrogel. Scale bars: 20 μm; magnification: 600×. (L) Relative proliferation rates of cells cultured on alginate, GelMA, collagen, and dSEM-HA hydrogels over a 5-day period (n = 8). (M) Gene Ontology classification bar chart categorizing the identified proteomic profiles of dSEM into biological processes, cellular components, and molecular functions. Notes: Data are presented as mean ± standard deviation. Statistical significance was determined using one-way analysis of variance followed by Newman–Keuls post hoc test. *p < 0.05, **p < 0.01, ***p < 0.001, and ****p < 0.0001.

enhanced wound closure rates over the observation period (Figure 1F), indicating the potent chemotactic and pro-migratory efficacy of the hBMSC-EVs.

3.3. Fabrication and biocompatibility of the 3D-printed dSEM-EV hydrogel

To construct a biomimetic microenvironment for EV delivery, a dSEM was derived from human skin tissues. LC–MS proteomics and subsequent bioinformatics analyses revealed that the dSEM is highly enriched in essential ECM components and signaling proteins (Figure 1G and 1M), which are known to facilitate fibroblast adhesion and proliferation. Following a sequential process of lyophilization, cryomilling, and solubilization (Figure 1H and 1J), the dSEM was then loaded with hBMSC-EVs to formulate a bioactive dSEM-EV hydrogel.

Scanning electron microscopy characterization demonstrated that the dSEM-EV hydrogel maintains a highly porous, interconnected microstructural topology similar to that of native skin tissue (Figure 1K). The biocompatibility of the composite hydrogel was evaluated using Live/Dead staining (Figure 1I) and CCK-8 proliferation assays (Figure 1L). The results confirmed that the dSEM-based environment supports excellent cell viability, with negligible cell death (PI-positive) observed. Over a 5-day culture period, cells encapsulated within the dSEM-HA hydrogel exhibited a robust, time-dependent exponential proliferation pattern, significantly outperforming conventional alginate, GelMA, or collagen-only hydrogels (Figure 1L).

Gene Ontology (GO) and Kyoto Encyclopedia of Genes and Genomes (KEGG) pathway enrichment analyses (Figure 1G and 1M) further elucidated the molecular basis for this bioactivity, revealing significant enrichment in biological processes associated with extracellular structure organization, cell adhesion molecule binding, and focal adhesion dynamics. These proteomic and transcriptomic signatures mechanistically suggest that the dSEM-based microenvironment synergizes with hBMSC-EVs to orchestrate the complex cascade of wound healing and tissue regeneration.

3.4. Rheological optimization and 3D bioprinting of the dSEM-EV hydrogel

To achieve high-fidelity additive manufacturing, the rheological properties of the dSEM-EV bio-ink were systematically evaluated. Oscillatory shear rheometry demonstrated that the bio-ink possessed optimal viscoelasticity and distinct shear-thinning behavior, which are prerequisites for smooth extrusion during the bioprinting process (Figure 2A). Macroscopic observations confirmed that the optimized bio-ink could be precisely extruded to fabricate highly ordered, self-supporting 3D macroscopic architectures with tailorable geometric patterns (e.g., rectilinear and triangular infills) and varying porosities (Figure 2B). Cell viability measurements further indicated that the printed hydrogel could maintain excellent cell biocompatibility (Figure 2C), creating a favorable microenvironment for subsequent cell viability and attachment. The cytocompatibility and biological inductive properties of the scaffolds were rigorously assessed. Live/Dead fluorescence staining revealed that cells encapsulated within the 3D-printed grids maintained near-complete viability (predominantly green fluorescence) immediately after printing (day 0). By day 3, the encapsulated cells exhibited robust morphological spreading and extensive cellular elongation along the printed struts, indicating excellent cell–matrix interactions (Figure 2D). Corresponding SEM morphological tracking corroborated these findings, visualizing extensive cellular anchorage and *de novo* ECM deposition on the scaffold surface over time (Figure 2E).

To elucidate the intrinsic molecular mechanisms by which the EV-loaded composite scaffold accelerates tissue repair, transcriptomic profiling and RT-qPCR were conducted. Hierarchical clustering heatmaps of the global gene expression profiles revealed that cells cultured within the hBMSC-EV-loaded scaffolds exhibited a transcriptomic signature remarkably homologous to that of native skin tissue, significantly bridging the *in vitro* gap (Figure 2F). Concurrently, GO and KEGG pathway enrichment analyses highlighted the robust activation of critical regenerative cascades. The differentially expressed genes were predominantly enriched in pathways governing ECM organization, focal adhesion, angiogenesis, and Wnt signaling (Figure 2G). RT-qPCR validation further confirmed that the EV-loaded scaffolds profoundly upregulated the expression of critical pro-regenerative and matrix remodeling genes, such as *Cdh2* (Figure 2H) and *Col1a1* (Figure 2I), while precisely modulating the expression of matrix metalloproteinases (*Mmp2*, *Mmp9*) (Figure 2J and 2K). This sustained bioactivity is supported by the cumulative protein release profile (Figure 2L), which demonstrates a steady, controlled liberation of dSEM-EVs from the scaffold over 7 days, providing the necessary temporal signaling to drive these regenerative gene expression patterns. These molecular insights comprehensively demonstrate that the synergistic delivery of dSEM and hBMSC-EVs structurally and biologically orchestrates the microenvironment toward optimal wound regeneration.

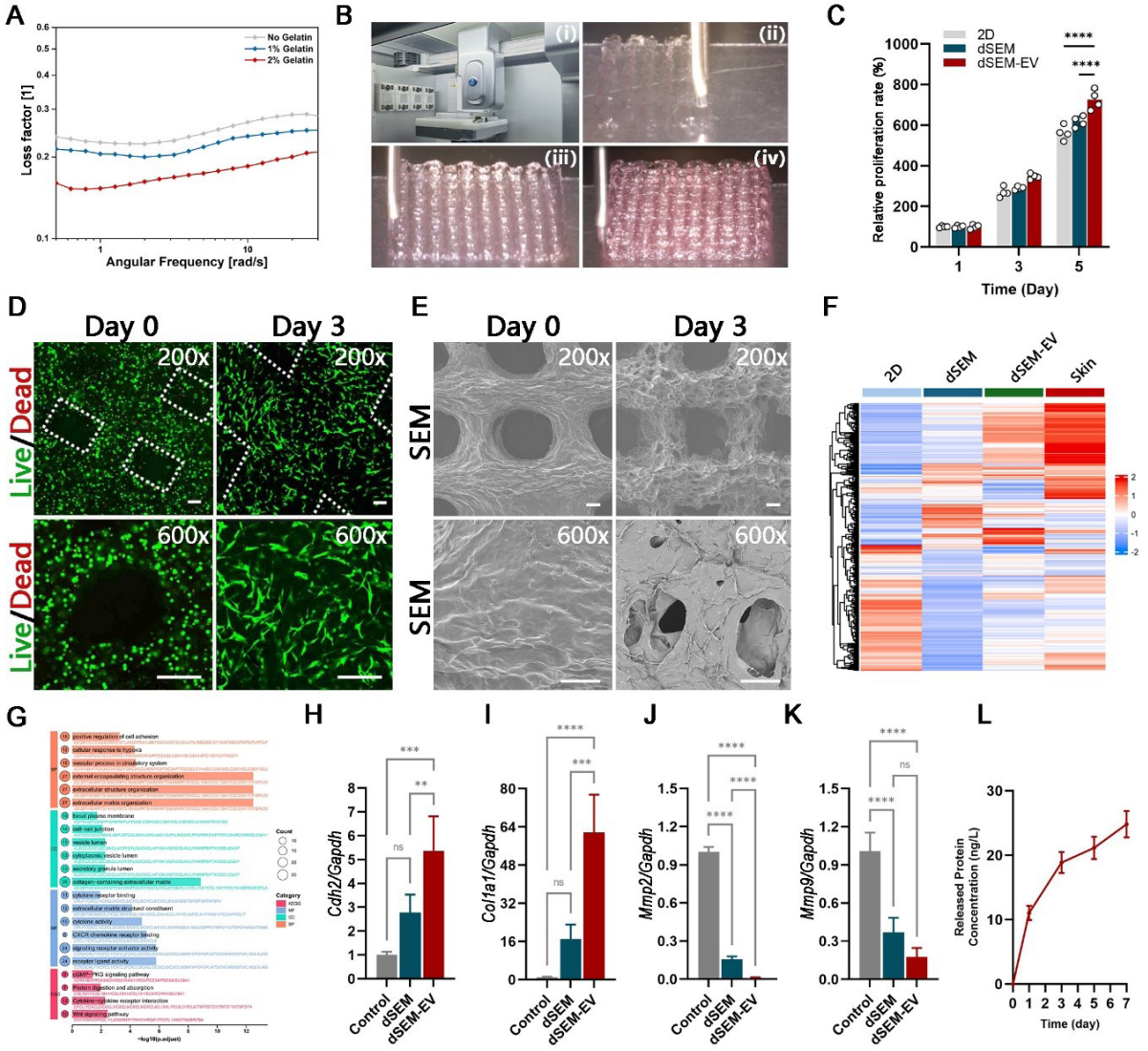

Figure 2. Rheological optimization, 3D bioprinting process, *in vitro* biocompatibility, and transcriptomic profiling of the human bone marrow mesenchymal stem cell-derived extracellular vesicle (hBMSC-EV)-loaded decellularized skin extracellular matrix (dSEM)-EV hydrogel scaffolds. (A) Rheological characterization detailing the dependence of the loss factor on angular frequency for bio-ink optimization (n = 3). (B) Sequential optical images (i–iv) illustrating the 3D bioprinting process of the formulated hydrogel into a highly ordered grid architecture. (C) Relative proliferation rates of target cells cultured in 2D cell culture plates, EV-free dSEM scaffolds, and hBMSC-EV-loaded dSEM-EV scaffolds evaluated over 5 days (n = 4). (D) Representative Live/Dead fluorescence micrographs of cells encapsulated within the 3D-bioprinted scaffolds at day 0 and day 3 (Green: viable cells; Red: dead cells). Scale bars: 100 µm/100 µm; magnification: 200×/600×. (E) Scanning electron microscopy images demonstrating the topological microstructure of the 3D-printed dSEM-EV scaffold at day 0 and day 3. Scale bars: 100 µm/100 µm; magnification: 200×/600×. (F) Hierarchical clustering heatmap of global transcriptomic profiles (RNA-seq) comparing cells in 2D culture, dSEM scaffolds, dSEM-EV scaffolds, and native skin tissue. (G) Bubble chart detailing the Gene Ontology and Kyoto Encyclopedia of Genes and Genomes pathway enrichment analysis, highlighting the activation of extracellular matrix organization, angiogenesis, and cell-matrix interactions. (H–K) Quantitative RT-qPCR analysis of pro-regenerative *Cdh2* (H), *Col1a1*(I), and matrix remodeling gene expressions *Mmp2* (J), *Mmp9* (K) in target cells subjected to different treatments (n = 3). Data are presented as mean ± standard deviation. (L) Cumulative protein release profile used as a surrogate measure of dSEM-EV release from the scaffold over 7 days. Statistical significance was determined using one-way analysis of variance followed by Newman–Keuls post hoc comparisons. *$p < 0.05$, **$p < 0.01$, ***$p < 0.001$, and ****$p < 0.0001$.

3.5. Fabrication, physicochemical characterization of the PCL–Cu_2O scaffold and the bilayer composite scaffold

Addressing the highly susceptible, multidrug-resistant bacterial microenvironment characteristic of chronic diabetic wounds necessitates a robust physical and chemical barrier. Consequently, the base PCL–Cu_2O scaffold was systematically engineered. Macroscopic evaluation confirmed that adjusting the fabrication parameters and printing gaps (100–1,000 μm) enabled precise control of scaffold porosity, ensuring an optimized permeability for gas exchange (Figure 3A–3D).

To elucidate the surface chemical composition, XPS was conducted. The high-resolution scanning of the Cu 2p orbitals unambiguously verified the chemical state of copper on the scaffold surface (Figure 3F). Furthermore, the physical properties and antimicrobial efficacy against MRSA were rigorously evaluated across varying Cu_2O concentrations (0–1.5%). Multi-dimensional characterization, including water contact angle measurements and SEM micrographs, illustrated the impact of copper loading on scaffold morphology (Figure 3E).

The bactericidal performance against MRSA and the corresponding cytocompatibility were specifically prioritized. Quantitative analysis of cell viability and antibacterial efficacy demonstrated a dose-dependent effect; while Cu_2O endowed the scaffold with potent bactericidal activity (indicated by representative agar plates), the Live/Dead staining of fibroblasts confirmed the concentration-dependent cytocompatibility (**F**Figure 3E, 3H, and 3I). Additionally, the cumulative release kinetics showed a sustained liberation of copper ions over a 14-day period (Figure 3G). Finally, the integrated asymmetric bilayer scaffold—comprising the 3D-printed dSEM-EV top layer and the electrospun PCL–Cu_2O base layer—was characterized via SEM, revealing a monolithic microarchitecture with functional spatial compartmentalization (Figure 3J).

3.6. *In vivo* synergistic evaluation of diabetic wound healing and tissue remodeling

To rigorously validate the translational potential of the composite Cu_2O-dSEM scaffold, an *in vivo* full-thickness skin defect model in diabetic mice was established (Figure 4A). Macroscopic digital tracking of the wound beds over a 20-day observation period (days 0, 5, 10, 15, and 20) revealed distinctly accelerated wound closure kinetics in the intervention groups. The composite Cu_2O-dSEM scaffold group exhibited the most profound reduction in residual wound area and the fastest healing rate, significantly outperforming the untreated control, the standalone Cu_2O barrier, and the standalone dSEM-EV hydrogel (Figure 4B and 4C).

Histopathological evaluations at day 20 via H&E and Masson's trichrome staining corroborated the macroscopic observations (Figure 4D). The composite scaffold promoted superior granulation tissue maturation and enhanced ECM deposition. Quantitative morphological analyses revealed a significantly higher relative collagen density and an optimized scar elevation index in the Cu_2O-dSEM group (Figure 4E and 4F), indicating functional tissue regeneration rather than fibrotic scar hyperplasia.

To further delineate the underlying *in vivo* regenerative mechanisms, comprehensive immunohistochemical profiling was performed. The composite scaffold induced a robust upregulation of CD31 (Figure 4G), signifying extensive neovascularization crucial for reperfusing the ischemic diabetic wound beds. Concurrently, heightened expressions of COL1 (Figure 4H) underscored accelerated ECM reconstruction and basement membrane maturation. The expression of pan-cytokeratin (panCK) (Figure 4I), hypoxia-inducible factor 1 alpha (HIF1α) (Figure 4J), vimentin (VIM) (Figure 4K), and laminin (LAM) (Figure 4L) further validated the enhanced re-epithelialization and fibroblast recruitment driven by the EV-loaded hydrogel. Collectively, these comprehensive *in vivo* findings unequivocally demonstrate the spatiotemporal synergistic effects of the bilayer composite scaffold in eradicating intractable infections, stimulating microangiogenesis, and orchestrating high-quality dermal regeneration.

4. Discussion

Chronic diabetic wounds represent a formidable clinical challenge, primarily characterized by persistent bacterial infections, impaired angiogenesis, oxidative stress, and a dysregulated inflammatory microenvironment that collectively impede the normal healing cascade.[34,35] Traditional wound dressings act as passive barriers and do not effectively target the complex pathological characteristics of diabetic wounds, such as the need for ongoing protection against infections and promotion of tissue regeneration.[36,37] To address this gap in treatment, we have developed a unique asymmetric bilayer composite scaffold. This scaffold consists of two distinct layers, a 3D-bioprinted dSEM-EV hydrogel top and an electrospun PCL–Cu_2O nanofibrous base layer. This design allows for the integration of both antimicrobial properties and tissue regeneration capabilities in a spatially and temporally controlled manner, leading to improved healing outcomes in chronic diabetic wounds. The dSEM-EV hydrogel top layer provides a supportive environment for cell growth and

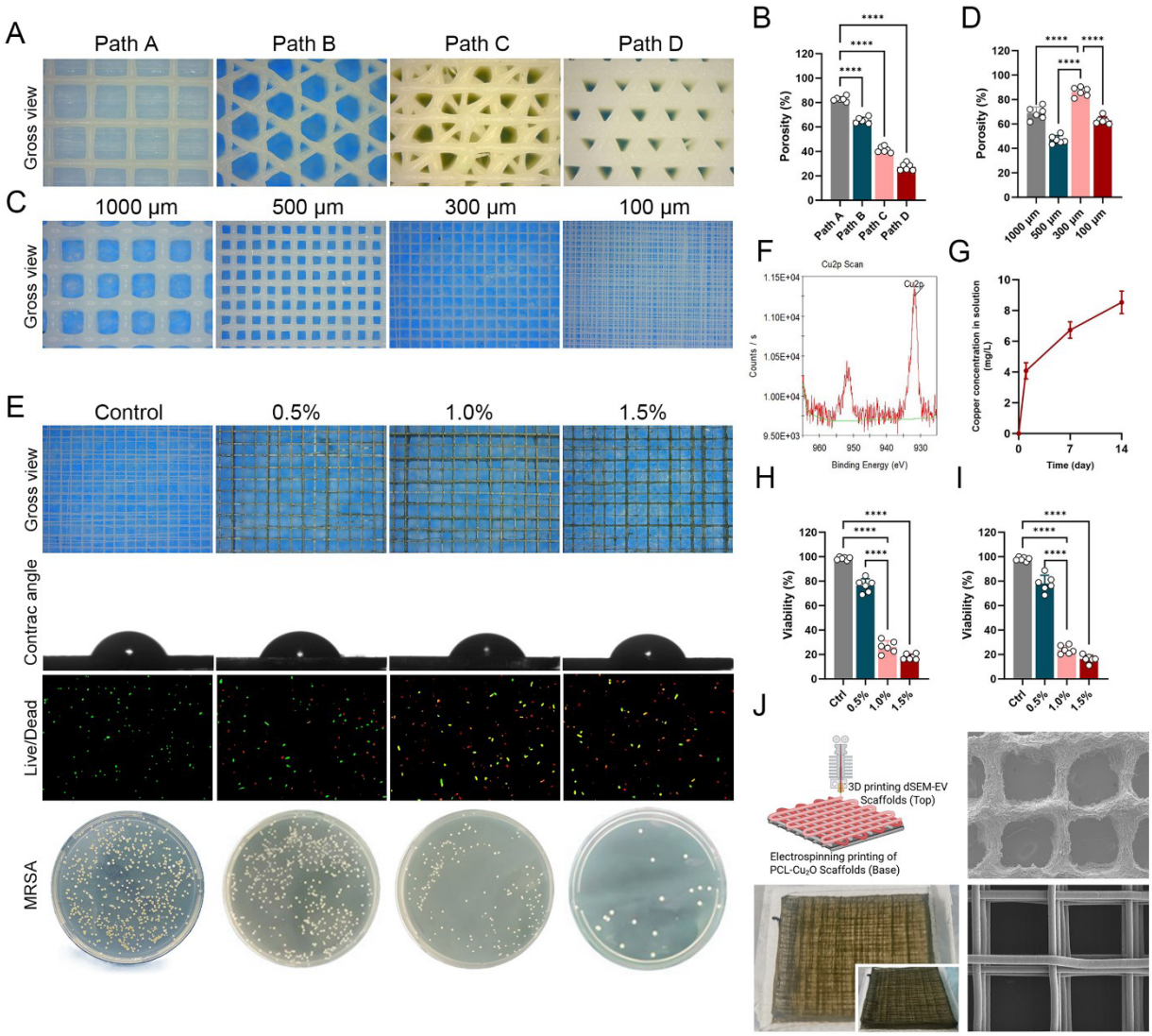

Figure 3. Structural characterization, Cu_2O loading optimization, and evaluation of antibacterial properties and cytocompatibility. (A, B) Gross morphology and quantitative porosity analysis of scaffolds fabricated using different printing paths (Paths A–D). (C, D) Visual appearance and porosity comparison of scaffolds with varied grid spacings (100–1,000 μm). (E) Multi-dimensional characterization of scaffolds with varying Cu_2O concentrations (0–1.5%): gross views, water contact angle measurements, Scanning electron microscopy (SEM) images, Live/Dead staining of fibroblasts, and representative agar plate images of methicillin-resistant *Staphylococcus aureus* (MRSA) colonies. (F) X-ray photoelectron spectroscopy Cu 2p high-resolution spectrum confirming the chemical state of copper on the scaffold surface. (G) Cumulative release kinetics of copper ions from the PCL–Cu_2O scaffold over a 14-day period. (H, I) Quantitative analysis of cell viability (H) and antibacterial efficacy against MRSA (I) showing the dose-dependent effects of Cu_2O. (J) Schematic illustration of the integrated asymmetric bilayer scaffold (3D-printed dSEM-EV top and electrospun PCL–Cu_2O base) with corresponding SEM characterization of the microarchitecture. Data are presented as mean ± standard deviation ($n = 3$). $^*p < 0.05$, $^{**}p < 0.01$, $^{***}p < 0.001$, $^{****}p < 0.0001$.

migration, promoting tissue regeneration. Meanwhile, the PCL–Cu_2O nanofibrous base layer acts as a barrier against bacterial infections, preventing further complications in the wound healing process. The combination of these two layers creates a synergistic effect, enhancing the overall healing potential of the scaffold. By targeting multiple aspects of diabetic wound pathology simultaneously, our novel scaffold aims to address the complex nature of chronic diabetic wounds and improve patient outcomes. With its unique design and multifunctional properties, this composite scaffold represents a promising advancement in the field of wound care, offering new possibilities for the treatment of challenging diabetic ulcers. The regenerative core of our composite scaffold relies fundamentally on the

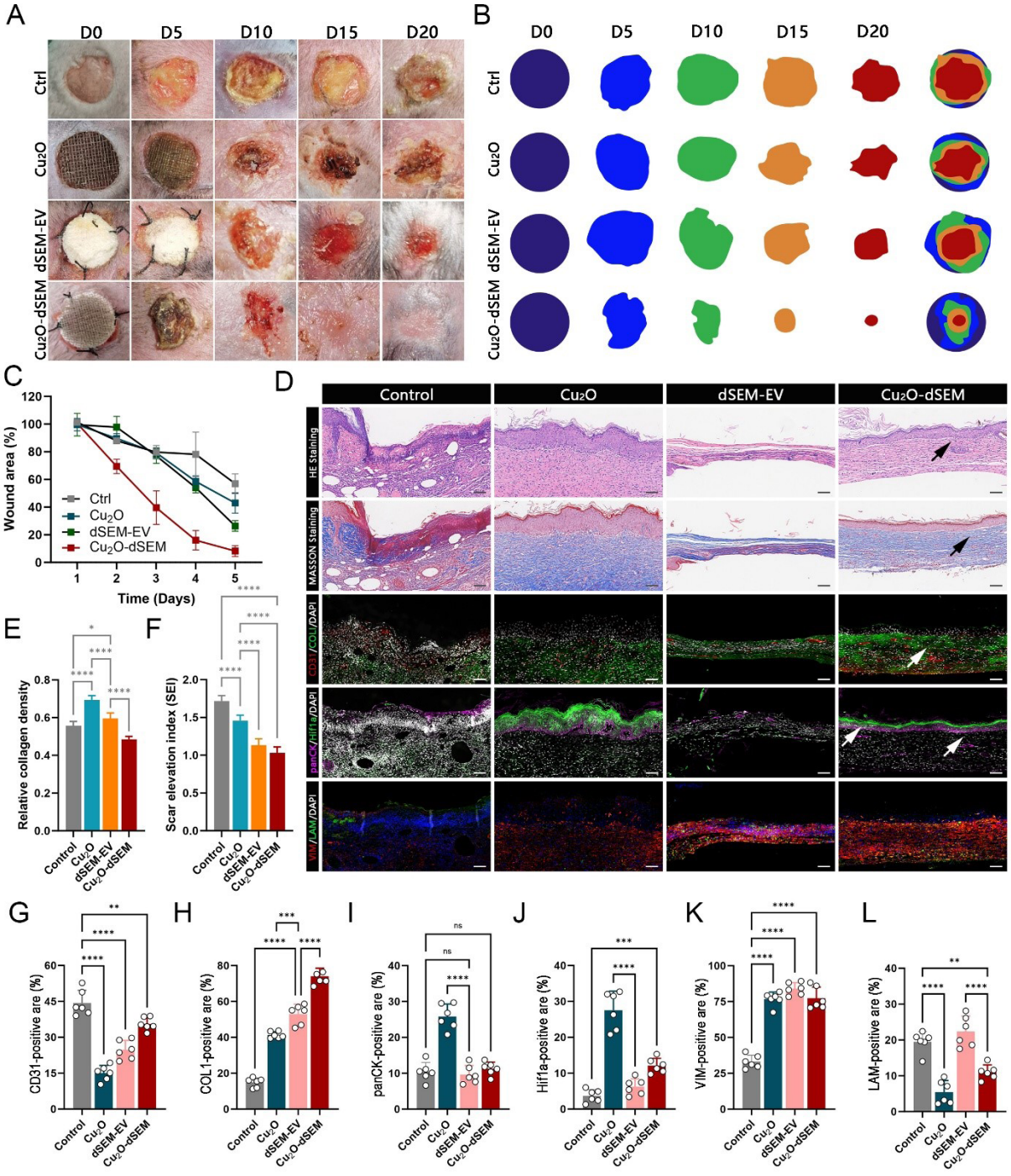

Figure 4. The asymmetric composite scaffold significantly accelerated wound closure *in vivo*. (A) Representative gross images of wounds in the Ctrl, Cu_2O, dSEM-EV, and Cu_2O-dSEM groups on days 0, 5, 10, 15, and 20. (B) Representative wound-area tracings/segmentation maps corresponding to panel A. (C) Quantification of wound area over time. (D) Representative histological and immunofluorescence images of wound tissues collected on day 20, including hematoxylin and eosin (H&E) staining, Masson's trichrome staining, and immunochemical (IHC) staining for the CD31, COL1, pan-cytokeratin (panCK), hypoxia-inducible factor 1 alpha (HIF-1α), vimentin (VIM), and laminin (LAM) in different groups on 20 days. (E) Relative collagen density and (F) scar elevation index among the groups (Ctrl, Cu_2O, dSEM-EV, and Cu_2O-dSEM) on day 20. (G–L) Quantification of CD31 (G), COL1 (H), panCK (I), HIF1a (J), VIM (K), and LAM (L) staining among the groups (Ctrl, Cu_2O, dSEM-EV, and Cu_2O-dSEM) on day 20. Statistical significance was determined using one-way analysis of variance followed by Newman–Keuls post hoc comparisons. $^*p < 0.05$, $^{**}p < 0.01$, $^{***}p < 0.001$, and $^{****}p < 0.0001$.

bioactive properties of hBMSC-EVs. Mesenchymal stem cells have been extensively documented to orchestrate tissue remodeling through paracrine mechanisms, releasing EVs enriched with proteins, lipids, and nucleic acids that modulate inflammatory cascades, promote angiogenesis, and suppress excessive fibrosis.[38,39] Functionally, hBMSC-EVs significantly enhanced fibroblast proliferation and migration in a concentration-dependent manner, corroborating their established role in promoting cellular events critical for wound re-epithelialization and granulation tissue formation.[40,41] These findings align with recent studies demonstrating that stem cell-derived EVs accelerate cutaneous wound healing by delivering pro-regenerative miRNAs and growth factors to recipient cells.[29,42]

In order to effectively deliver bioactive EVs and create a supportive environment for the recruitment of endogenous cells, we utilized a dSEM hydrogel as the top scaffold layer. The dSEM has been demonstrated to maintain crucial components of the ECM, such as collagen and glycosaminoglycans, which play a vital role in cellular adhesion, proliferation, and matrix restructuring.[18] Through our extensive transcriptomic analysis, we discovered that the dSEM environment significantly enhanced biological processes related to ECM organization, cell adhesion molecule binding, and focal adhesion dynamics. These findings underscored the notable activation of pathways associated with angiogenesis and inflammatory modulation, illustrating how the biomimetic qualities of the dSEM work in harmony with hBMSC-EV cargo to facilitate effective wound healing. These results align with previous studies showing that ECM-derived hydrogels offer more favorable environments for cell survival and function compared to synthetic polymer matrices.[43,44]

In addition to promoting tissue regeneration, effective management of the highly susceptible, multidrug-resistant bacterial microenvironment in diabetic wounds necessitates a robust physical and chemical barrier.[45] To address this need, we systematically engineered a base electrospun PCL–Cu_2O layer. Our previous research has shown that these electrospun nanofibers have controlled porosity and spatial alignment, allowing for adequate gas exchange and providing chemotactic cues to potentially accelerate re-epithelialization.[13,46] A key feature of the Cu_2O-doped scaffold is its potent antibacterial activity against MRSA, a common pathogen in chronic wounds that can lead to serious complications. This antibacterial effect is believed to be due to the release of copper ions, which create reactive oxygen species and disrupt bacterial membrane integrity.[47-49] The bilayer architecture, with dense electrospun nanofibrous membrane seamlessly adhered to the highly porous 3D-printed dSEM-EV matrix, provided both structural integrity and dual-functional spatial compartmentalization essential for coordinated infection control and tissue regeneration.

Our composite scaffold was tested for its therapeutic effectiveness in treating full-thickness skin defects in diabetic mice with impaired healing, a model similar to human diabetic wounds. Immunohistochemical analysis provided insights into the regenerative processes occurring *in vivo*. The scaffold promoted the growth of new blood vessels, as evidenced by increased levels of CD31, which is essential for improving blood flow to ischemic diabetic wounds. This is consistent with the known pro-angiogenic properties of both hBMSC-EVs and dSEM components,[50,51] Heightened collagen type I expression suggested enhanced ECM deposition and remodeling, whereas increased laminin expression supported improved basement-membrane maturation. Enhanced expression of panCK and VIM validated improved re-epithelialization and fibroblast recruitment driven by the EV-loaded hydrogel, while upregulated LAM suggested improved dermal–epidermal junction integrity. The modulation of HIF-1α expression indicated potential involvement of hypoxia-responsive pathways in the observed angiogenic response, aligning with previous reports linking EV-mediated HIF-1α regulation to wound healing.[52]

Importantly, the anti-inflammatory properties observed in our study warrant further discussion. Macrophage polarization from the pro-inflammatory M1 phenotype to the pro-regenerative M2 phenotype represents a critical checkpoint in the transition from inflammation to proliferation during wound healing.[53,54] While our current investigation did not extensively characterize macrophage responses, the transcriptomic signatures of dSEM-EV scaffolds revealed significant enrichment of pathways related to inflammatory modulation. It is well-established that persistent M1 polarization can lead to chronic inflammation in diabetic wounds.[55] Therefore, it is important for future studies to systematically investigate whether our composite scaffold can promote M2 polarization. This may involve mechanisms that interact with the NF-κB pathway, as seen in recent studies on immunomodulatory hydrogel systems.[56,57] Such investigations would provide a deeper mechanistic understanding and potentially reveal additional therapeutic targets.

Several limitations of this study should be acknowledged. First, while we demonstrated the antibacterial efficacy of PCL–Cu_2O against MRSA, a comprehensive evaluation against polymicrobial biofilms commonly encountered in chronic wounds would strengthen clinical translatability.[58] Second, the long-term fate of implanted scaffolds, including

degradation kinetics and potential toxicity of degradation byproducts, requires extended *in vivo* observation. Third, although we employed a clinically relevant diabetic mouse model, larger animal studies with wound geometries more closely mimicking human pathophysiology would provide additional preclinical validation.[59] Fourth, the precise molecular mechanisms by which hBMSC-EVs and dSEM synergistically promote angiogenesis and modulate inflammation warrant further elucidation through targeted signaling pathway inhibition studies.

5. Conclusion

In this study, we successfully developed an asymmetric bilayer composite scaffold integrating 3D-bioprinted dSEM-EV hydrogel with electrospun PCL–Cu_2O nanofibers, which structurally mimics native skin architecture. The top dSEM-EV layer exhibited excellent biocompatibility and bioactivity, significantly promoting fibroblast proliferation and migration through activation of ECM organization and angiogenesis-related pathways. The base PCL–Cu_2O layer provided robust antibacterial activity against MRSA, effectively addressing the persistent infection challenge in diabetic wounds. *In vivo* evaluation in a db/db diabetic mouse model demonstrated that the composite scaffold significantly accelerated wound closure, promoted neovascularization, enhanced collagen deposition, and facilitated re-epithelialization compared to standalone treatments. Accordingly, this study introduces a novel strategy that combines 3D bioprinting and electrospinning technologies to engineer a multifunctional scaffold with spatiotemporal "anti-infection and pro-regeneration" synergy, specifically designed to tackle the complex microenvironment of chronic diabetic wounds, thereby providing a basis for further development of advanced wound-management strategies.

Acknowledgments

None.

Funding

This work was supported by the grants from the National Key R&D Program of China (No. 2023YFC2411303) and the National Natural Science Foundation of China (Grant No. 82402819, 82402940).

Conflict of interest

Yongqiang Hao serves as the guest editor of the special issue, but did not in any way involve in the editorial and peer-review process conducted for this paper, directly or indirectly. Other authors declare they have no competing interests.

Author contributions

Conceptualization: Chenyu Zhang, Zuyan Lu, Yongqiang Hao
Formal analysis: Zuyan Lu
Investigation: Lei Pan, Yuan Fang
Methodology: Hongyu Chen, Yu Han, Qiang Wu, Ye Sun
Writing–original draft: Chenyu Zhang, Zuyan Lu
Writing–review & editing: Quan Hu, Yuanyuan Liu

Ethics approval and consent to participate

The collection and use of human skin tissue were approved by the Ethics Committee of Shanghai Ninth People's Hospital (Approval No. SH9H-2021-T401-4), and informed consent was obtained from all donors. All animal experiments in this study were approved by the Institutional Animal Care and Use Committee (IACUC) of Shanghai Ninth People's Hospital (Approval No. SH9H-2024-A660-SB). All procedures were performed in accordance with the Guide for the Care and Use of Laboratory Animals.

Consent for publication

Not applicable.

Availability of data

All data are available in the manuscript.

References

1. Slominski A, Wortsman J. Neuroendocrinology of the skin. *Endocr Rev*. 2000;21(5):457-487.

   doi: 10.1210/edrv.21.5.0410

2. Proksch E, Brandner JM, Jensen JM. The skin: an indispensable barrier. *Exp Dermatol*. 2008;17(12):1063-1072.

   doi: 10.1111/j.1600-0625.2008.00786.x

3. Sen CK. Human Wound and Its Burden: Updated 2020 Compendium of Estimates. *Adv Wound Care (New Rochelle)*. 2021;10(5):281-292.

   doi: 10.1089/wound.2021.0026

4. Armstrong DG, Boulton AJM, Bus SA. Diabetic Foot Ulcers and Their Recurrence. *N Engl J Med*. 2017;376(24):2367-2375.

   doi: 10.1056/NEJMra1615439

5. Jones RE, Foster DS, Longaker MT. Management of Chronic Wounds-2018. *JAMA*. 2018;320(14):1481-1482.

   doi: 10.1001/jama.2018.12426

6. Morton LM, Phillips TJ. Wound healing and treating wounds: Differential diagnosis and evaluation of chronic

wounds. *J Am Acad Dermatol*. 2016;74(4):589-605.

doi: 10.1016/j.jaad.2015.08.068

7. Fu X. Wound healing center establishment and new technology application in improving the wound healing quality in China. *Burns Trauma*. 2020;8:tkaa038.

doi: 10.1093/burnst/tkaa038

8. Jiang Y, Huang S, Fu X, *et al*. Epidemiology of chronic cutaneous wounds in China. *Wound Repair Regen*. 2011;19(2):181-188.

doi: 10.1111/j.1524-475X.2010.00666.x

9. Wang Q, Luo Z, Li Z, *et al*. In-situ oxygen-supplying ROS nanopurifier for enhanced healing of MRSA-infected diabetic wounds via microenvironment modulation. *Acta Biomater*. 2025;193:334-347.

doi: 10.1016/j.actbio.2024.12.044

10. Lu Y, Xu J, Su Y, *et al*. A biocompatible double-crosslinked gelatin/sodium alginate/dopamine/quaternized chitosan hydrogel for wound dressings based on 3D bioprinting technology. *Int J Bioprint*. 2023;9(2):689.

doi: 10.18063/ijb.689

11. Fang H, Xu J, Ma H, *et al*. Functional materials of 3D bioprinting for wound dressings and skin tissue engineering applications: A review. *Int J Bioprint*. 2023;9(5):757.

doi: 10.18063/ijb.757

12. Mao S, Man J, Wang J, *et al*. Research progress and challenges of bioprinting in wound dressing and healing: Bibliometrics-based analysis and perspectives. *Int J Bioprint*. 2023;9(2):653.

doi: 10.18063/ijb.v9i2.653

13. Keirouz A, Chung M, Kwon J, Fortunato G, Radacsi N. 2D and 3D electrospinning technologies for the fabrication of nanofibrous scaffolds for skin tissue engineering: A review. *Wiley Interdiscip Rev Nanomed Nanobiotechnol*. 2020;12(4):e1626.

doi: 10.1002/wnan.1626

14. Wang X, Wang Y, Teng Y, *et al*. 3D bioprinting: opportunities for wound dressing development. *Biomed Mater*. 2023;18(5):052001.

doi: 10.1088/1748-605X/ace228

15. D A G, Adhikari J, Debnath P, Ghosh S, *et al*. 3D printing of bacterial cellulose for potential wound healing applications: Current trends and prospects. *Int J Biol Macromol*. 2024;279:135213.

doi: 10.1016/j.ijbiomac.2024.135213

16. Han Y, Lian M, Zhang C, *et al*. Study on bioactive PEGDA/ECM hybrid bi-layered hydrogel scaffolds fabricated by electro-writing for cartilage regeneration. *Appl Mater Today*. 2022;28:101547.

doi: 10.1016/j.apmt.2022.101547

17. Xu J, Yang S, Su Y, *et al*. A 3D bioprinted tumor model fabricated with gelatin/sodium alginate/decellularized extracellular matrix bioink. *Int J Bioprint*. 2023;9(1):630.

doi: 10.18063/ijb.v9i1.630

18. Malta MD, Cerqueira MT, Marques AP. Extracellular matrix in skin diseases: The road to new therapies. *J Adv Res*. 2023;51:149-160.

doi: 10.1016/j.jare.2022.11.008

19. Durr HA, Abri S, Salinas SD, *et al*. Extracellular matrix repair and organization of chronic infected diabetic wounds treated with methacrylated chitosan-based hydrogels. *Acta Biomater*. 2025;199:166-177.

doi: 10.1016/j.actbio.2025.04.062

20. Song YT, Liu PC, Zhou XL, *et al*. Extracellular matrix-based biomaterials in burn wound repair: A promising therapeutic strategy. *Int J Biol Macromol*. 2024;283:137633.

doi: 10.1016/j.ijbiomac.2024.137633

21. Rueda-Gensini L, Serna JA, Cifuentes J, Cruz JC, Munoz-Camargo C. Graphene Oxide-Embedded Extracellular Matrix-Derived Hydrogel as a Multiresponsive Platform for 3D Bioprinting Applications. *Int J Bioprint*. 2021;7(3):353.

doi: 10.18063/ijb.v7i3.353

22. Lu Z, Miao X, Zhang C, *et al*. An osteosarcoma-on-a-chip model for studying osteosarcoma matrix-cell interactions and drug responses. *Bioact Mater*. 2024;34:1-16.

doi: 10.1016/j.bioactmat.2023.12.005

23. Lu Z, Jiang W, Zhao W, Zhao J, Dai K. Fabrication of 3D matrix microenvironment by two-photon lithography for mechanobiology study. *Mechanobiol Med*. 2023;1(1):100010.

doi: 10.1016/j.mbm.2023.100010

24. Carranza T, Uranga J, Irastorza A, *et al*. Combination of 3D printing and electrospinning to develop chitin/gelatin/PVA scaffolds. *Int J Bioprint*. 2023;9(3):701.

doi: 10.18063/ijb.701

25. Luo Y, Li D, Lin C, *et al*. 3D bioprinting of mechanically graded GelMA hydrogels with tri-layered vascularized architecture for full-thickness skin regeneration. *Int J Bioprint*. 2025;11(4):328-349.

doi: 10.36922/ijb025090069

26. Zhang C, Ma P, Qin A, *et al*. Current Immunotherapy Strategies for Rheumatoid Arthritis: The Immunoengineering and Delivery Systems. *Research (Wash D C)*. 2023;6:0220.

doi: 10.34133/research.0220

27. Wang Y, Kong B, Chen X, *et al*. BMSC exosome-enriched acellular fish scale scaffolds promote bone regeneration. *J Nanobiotechnology*. 2022;20(1):444.

doi: 10.1186/s12951-022-01646-9

28. Su X, Yang J, Xu Z, *et al*. Fibrous scaffolds loaded with BMSC-derived apoptotic vesicles promote wound healing by inducing macrophage polarization. *Genes Dis*. 2025;12(2):101388.

doi: 10.1016/j.gendis.2024.101388

29. Wu J, Li S, Wang H, *et al*. High-yield BMSC-derived exosomes by the 3D culture system to enhance the skin wound repair. *Regen Biomater*. 2025;12:rbaf022.

doi: 10.1093/rb/rbaf022

30. Selvam S, Midhun BT, Bhowmick T, Chandru A. Bioprinting of exosomes: Prospects and challenges for clinical applications. *Int J Bioprint*. 2023;9(2):690.

doi: 10.18063/ijb.690

31. Han L, Liu Z, Li M, *et al*. 3D bioprinting of a dermal scaffold for full-thickness skin tissue regeneration. *Bio-Des Manuf*. 2025;8(1):68-84.

doi: 10.1631/bdm.2400058

32. Abaci A, Guvendiren M. Designing Decellularized Extracellular Matrix-Based Bioinks for 3D Bioprinting. *Adv Healthc Mater*. 2020;9(24):e2000734.

doi: 10.1002/adhm.202000734

33. Zhao H, Yang Y, An J, *et al*. Cu2O Nanocubes Embedded in Polycaprolactone Nanofibers for Photo–chemotherapeutic Wound Disinfection and Regeneration. *ACS Appl Nano Mater*. 2024;7(15):17707-17718.

doi: 10.1021/acsanm.4c02928

34. Falanga V. Wound healing and its impairment in the diabetic foot. *Lancet*. 2005;366(9498):1736-1743.

doi: 10.1016/S0140-6736(05)67700-8

35. Brem H, Tomic-Canic M. Cellular and molecular basis of wound healing in diabetes. *J Clin Invest*. 2007;117(5):1219-1222.

doi: 10.1172/JCI32169

36. Liang Y, He J, Guo B. Functional Hydrogels as Wound Dressing to Enhance Wound Healing. *ACS Nano*. 2021;15(8):12687-12722.

doi: 10.1021/acsnano.1c04206

37. Zeng Q, Qi X, Shi G, Zhang M, Haick H. Wound Dressing: From Nanomaterials to Diagnostic Dressings and Healing Evaluations. *ACS Nano*. 2022;16(2):1708-1733.

doi: 10.1021/acsnano.1c08411

38. Liu C, Cheng C, Cheng K, *et al*. Precision exosome engineering for enhanced wound healing and scar revision. *J Transl Med*. 2025;23(1):578.

doi: 10.1186/s12967-025-06578-0

39. Rani S, Ryan AE, Griffin MD, Ritter T. Mesenchymal Stem Cell-derived Extracellular Vesicles: Toward Cell-free Therapeutic Applications. *Mol Ther*. 2015;23(5):812-823.

doi: 10.1038/mt.2015.44

40. Shabbir A, Cox A, Rodriguez-Menocal L, Salgado M, Van Badiavas E. Mesenchymal Stem Cell Exosomes Induce Proliferation and Migration of Normal and Chronic Wound Fibroblasts, and Enhance Angiogenesis In Vitro. *Stem Cells Dev*. 2015;24(14):1635-1647.

doi: 10.1089/scd.2014.0316

41. Zhang J, Guan J, Niu X, *et al*. Exosomes released from human induced pluripotent stem cells-derived MSCs facilitate cutaneous wound healing by promoting collagen synthesis and angiogenesis. *J Transl Med*. 2015;13:49.

doi: 10.1186/s12967-015-0417-0

42. Zhang S, Lu C, Zheng S, Hong G. Hydrogel loaded with bone marrow stromal cell-derived exosomes promotes bone regeneration by inhibiting inflammatory responses and angiogenesis. *World J Stem Cells*. 2024;16(5):499-511.

doi: 10.4252/wjsc.v16.i5.499

43. Bae M, Kim JJ, Kim J, Cho DW. Decellularized extracellular matrix for three-dimensional bioprinted in vitro disease modeling. *Int J Bioprint*. 2024;10(2):1970.

doi: 10.36922/ijb.1970

44. Liu W, Gao R, Yang C, *et al*. ECM-mimetic immunomodulatory hydrogel for methicillin-resistant Staphylococcus aureus-infected chronic skin wound healing. *Sci Adv*. 2022;8(27):eabn7006.

doi: 10.1126/sciadv.abn7006

45. Fu H, Zhang D, Zeng J, *et al*. Application of 3D-printed tissue-engineered skin substitute using innovative biomaterial loaded with human adipose-derived stem cells in wound healing. *Int J Bioprint*. 2023;9(2):674.

doi: 10.18063/ijb.v9i2.674

46. Dong R, Li Y, Chen M, *et al*. In Situ Electrospinning of Aggregation-Induced Emission Nanofibrous Dressing for Wound Healing. *Small Methods*. 2022;6(5):e2101247.

doi: 10.1002/smtd.202101247

47. Lipsky BA, Hoey C. Topical antimicrobial therapy for treating chronic wounds. *Clin Infect Dis*. 2009;49(10):1541-1549.

doi: 10.1086/644732

48. Pino PAO, Bosco FAO, Mollea C, Onida BAO. Antimicrobial Nano-Zinc Oxide Biocomposites for Wound Healing Applications: A Review. *Pharmaceutics*. 2023;15(3):970.

doi: 10.3390/pharmaceutics15030970

49. Chatterjee AK, Chakraborty R, Basu T. Mechanism of antibacterial activity of copper nanoparticles. *Nanotechnology*. 2014;25(13):135101.

doi: 10.1088/0957-4484/25/13/135101

50. Zeng X, Gan J, Huang D, Zhao Y, Sun L. Recombinant human collagen hydrogels with different stem cell-derived exosomes encapsulation for wound treatment. *J Nanobiotechnology*. 2025;23(1):241.

doi: 10.1186/s12951-025-03319-9

51. Sheng Z, Fu X, Cai S, *et al*. Regeneration of functional sweat gland-like structures by transplanted differentiated bone marrow mesenchymal stem cells. *Wound Repair Regen*. 2009;17(3):427-435.

doi: 10.1111/j.1524-475X.2009.00474.x

52. Deng C, Dong K, Liu Y, *et al*. Hypoxic mesenchymal stem cell-derived exosomes promote the survival of skin flaps after ischaemia-reperfusion injury via mTOR/ULK1/FUNDC1 pathways. *J Nanobiotechnology*. 2023;21(1):340.

doi: 10.1186/s12951-023-02098-5

53. Zhou S, Zhang X, Ni W, *et al*. An Immune-Regulating Polysaccharide Hybrid Hydrogel with Mild Photothermal Effect and Anti-Inflammatory for Accelerating Infected Wound Healing. *Adv Healthc Mater*. 2024;13(20):e2400003.

doi: 10.1002/adhm.202400003

54. Krzyszczyk P, Schloss R, Palmer A, Berthiaume F. The Role of Macrophages in Acute and Chronic Wound Healing and Interventions to Promote Pro-wound Healing Phenotypes. *Front Physiol*. 2018;9:419.

doi: 10.3389/fphys.2018.00419

55. Mirza RE, Fang MM, Ennis WJ, Koh TJ. Blocking interleukin-1beta induces a healing-associated wound macrophage phenotype and improves healing in type 2 diabetes. *Diabetes*. 2013;62(7):2579-2587.

doi: 10.2337/db12-1450

56. Chen T, Zhang X, Zhou S, *et al*. A versatile and double cross-linked hydrogel with potent antibacterial and immunomodulatory Zn@Met nanocomplexes for enhanced diabetic-infected wound healing. *Chem Eng J*. 2025;516:163942.

doi: 10.1016/j.cej.2025.163942

57. Xu N, Gao Y, Li Z, *et al*. Immunoregulatory hydrogel decorated with Tannic acid/Ferric ion accelerates diabetic wound healing via regulating Macrophage polarization. *Chem Eng J*. 2023;466:143173.

doi: 10.1016/j.cej.2023.143173

58. Zhao G, Usui ML, Lippman SI, *et al*. Biofilms and Inflammation in Chronic Wounds. *Adv Wound Care (New Rochelle)*. 2013;2(7):389-399.

doi: 10.1089/wound.2012.0381

59. Sullivan TP, Eaglstein WH, Davis SC, Mertz P. The pig as a model for human wound healing. *Wound Repair Regen*. 2001;9(2):66-76.

doi: 10.1046/j.1524-475x.2001.00066.x